Progress In Electromagnetics Research M, Vol. 72, 1–11, 2018

Spectral Behaviour of Planar Optical Waveguides and Microchannels in Cascade: Theoretical Evaluation

José R. García* **and Adrián F. Gavela**

Abstract—This paper presents an extension and update of a theoretical procedure developed by the authors for the determination of the electromagnetic waves scattering at interfaces between dielectric waveguides in cascade. The theoretical core of the problem is based on the generalized scattering matrix concept, together with the generalized telegraphist equations formulism and modal matching technique. The new version includes the following updates: a) possibility of using any material as waveguide cover, b) inclusion of alternating microchannels with optical waveguides, and c) possibility of analyzing periodic structures of segmented optical waveguides for sensing applications. The spectral results obtained for modulus and phase of the reflection and transmission coefficients have shown the potentiality of the new proposal in the scientific topics of photonic crystals, refractive index sensors and optical biosensors.

1. INTRODUCTION

Multiple discontinuities in dielectric waveguides, waveguide gratings and waveguide photonic crystals are widely studied in order to design, improve and optimize the flow of light as well as its applications in the design of microwave and integrated photonic devices. At microwave and optical frequencies, an extensive list of integrated devices were designed by using periodic structures: power dividers and filters, electromagnetic and photonic band gaps structures, optical switches and optical resonant microcavities as well as optical sensors and quantum dot lasers are typical examples [1–26]. On the other hand, segmented optical waveguides are periodic mediums which were widely studied, both from the electromagnetic propagation point of view [27–32] as well as their technological applications [33–37].

In a previous paper [1], a theoretical procedure that allows to know the electromagnetic behaviour of arbitrary dielectric waveguides connected both abruptly and gradually was described in detail. The electromagnetic scattering properties of cascade discontinuities between dielectric waveguides were obtained by using the Generalized Scattering Matrix (GSM) concept, together with the Generalized Telegraphist Equations (GTE) formulism and the Modal Matching Technique (MMT). The efficiency of the theoretical development was confirmed by the experimental results, both at microwave and optical frequencies.

In the present work, we focus our attention on the design of integrated optical periodic devices for sensing applications. For this reason, the theoretical algorithm described in [1] was extended and modified in order to make possible both the inclusion of any material as cover of the optical waveguides in cascade and the inclusion of microchannels as part of the complete device. In this way, the fact of being able to use any type of material (solid, fluid or gas) as cover in the waveguides as well as engraved microchannels, allows not only the design of optical refractive index sensors, but also the design of biosensors based in the presence of two simultaneous phenomenon: the cover evanescent field and the electromagnetic scattering at the periodic optical waveguides interfaces.

Received 4 June 2018, Accepted 28 July 2018, Scheduled 8 August 2018
* Corresponding author: José Rodríguez García (jose@uniovi.es).
The authors are with the Physics Department, University of Oviedo, Oviedo, Asturias 33007, Spain.

The new algorithm was applied to compute the generalized scattering coefficients (modulus and phase) which give the spectral performance of the device. Planar waveguide photonic crystals, with different cover materials and including local defects, and optical waveguide sensors with a variable number of microchannels were analysed. The obtained results show that multiple photonic band gaps can be obtained for the same photonic crystal configuration so that the introduction of a lattice defect creates an optical microcavity in each band gap. Besides, the cover refraction index influences the wavelength intervals where the different band gaps appear. Finally, the computed spectral results have shown the potentiality of this proposal in the subject of refractive index sensors and optical biosensors implemented with integrated optical waveguides and engraved microchannels.

2. THEORY

The first mathematical formulation of the problem was presented in [1], where the cover of the planar and channel optical waveguides was restricted to air. In the present work and in order to analyze in depth the influence of the cover refraction index, the procedure was reformulated. This new consideration is very important in order to analyze optical sensors based both on evanescent field interaction and electromagnetic field scattering. Consequently, in the new algorithm, the refraction index profile of an integrated planar optical waveguide (1-D), as shown in Figure 1(a), is written in the form:

$$n(y) = \begin{cases} n_c, & cover \\ n_s + \Delta n \cdot f\left(-\dfrac{y}{h}\right), & core \\ n_s, & substrate \end{cases} \tag{1}$$

In Equation (1), n_s represents the refractive index of the optical waveguide substrate; Δn refers to the maximum refractive index increment in the core region; f is the refraction index function along y direction, and h is the diffusion depth. Notice that, in this occasion, the refraction index of the cover, n_c, can take arbitrary values, unlike before algorithm where $n_c = 1$.

As shown in [1], the electromagnetic behaviour of periodical configurations in dielectric waveguides can be found through the following protocol:

a) Optical waveguides proper modes analysis: GTE formulation provides surface, fast and evanescent proper modes solutions.

b) GSM evaluation of single and multiple discontinuities: MMT procedure and a matrix connection algorithm provide the GSM of the complete structure.

Figure 1(a) is a side view of an abrupt discontinuity between two dielectric waveguides enclosed by perfectly conducting boundaries. The shielded dielectric waveguides, a and b, are located at $z < 0$ and $z > 0$, respectively, of the abrupt discontinuity, at $z = 0$.

The application of the MMT requires the previous evaluation of the planar optical waveguides proper modes. Slab and planar optical waveguides (1-D) propagate TE and TM proper modes [1]. Assuming optical waveguides free from losses, small variations of the index of refraction and propagation along the z axis of the form $\exp[j(\omega t - \beta z)]$, the following two dimensional Helmholtz's equation describes the propagation of the electromagnetic field in the planar optical waveguide and in terms of the vector electric field $\vec{E}$:

$$\nabla_t^2 \vec{E} + \left[k_0^2 n^2(y) - \beta^2\right] \vec{E} = \vec{0} \tag{2}$$

where k_0 represents the free space wavenumber, β the phase constant in the propagation direction z, and $n(y)$ the refraction index profile. We assume x and y as the horizontal and vertical coordinates, respectively.

As we are interested in 1-D dielectric waveguides, there is no variation in the x direction, and perfectly conducting parallel plates are used as shielding. To simulate the refractive index profile functions, the dielectric waveguide cross section is modelled by a mesh of pixels with different refractive index values, as shown in Figure 1(b). Arbitrary fine meshes can be used in order to optimize the refractive index function. As explained in [1], the method can be applied successfully to 1-D and 2-D optical waveguides proper modes analysis as well as the study of any dielectric configuration modelled as a cascaded set of abrupt discontinuities.

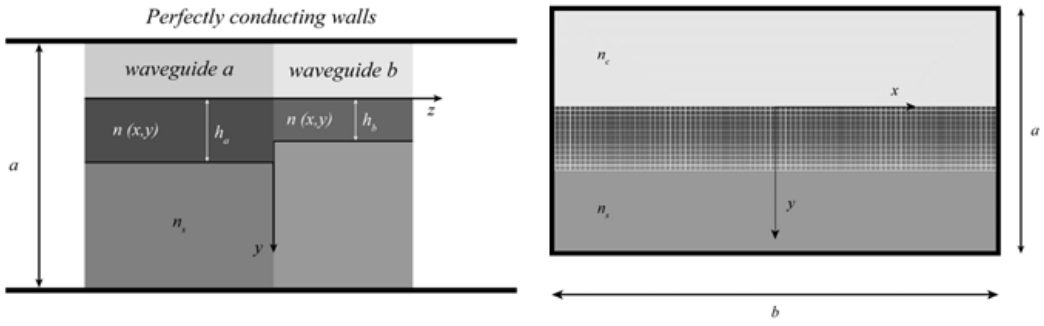

(a) (b)

Figure 1. (a) Side view of two shielded planar optical waveguides connected by an abrupt transition. (b) Cross section of a shielded planar optical waveguide modelled by a grid of pixels with different refractive indices.

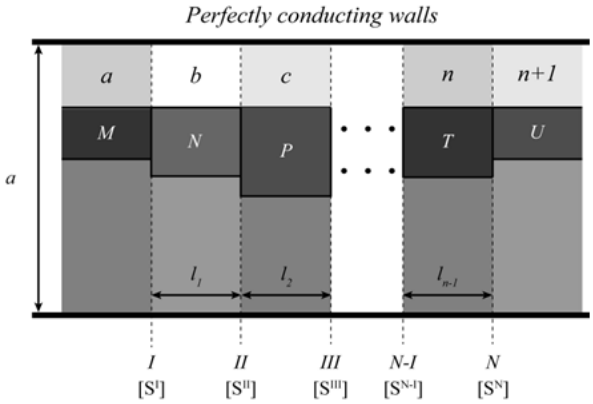

Figure 2. General representation of a cascaded set of N abrupt discontinuities in shielded dielectric waveguides.

Figure 2 shows a scheme of multiple cascaded discontinuities. The labels $a, b, c \ldots n+1$ denote optical waveguides order, and the number of waveguide proper modes is labeled by M, N, P, $\ldots U$, whereas the waveguide lengths are l_i (i =1, 2, 3, $\ldots$, $n-1$). As we can see, $n+1$ interconnected optical waveguides provide n cascade discontinuities. Once the proper modes of each individual planar optical waveguide were evaluated and selected [1], the application of the MMT strategy to each discontinuity to obtain its GSM is possible [1]. Finally, the total GSM, $[S^T]$, of the cascaded set of abrupt discontinuities can be obtained by joining the **N** GSM's, resulting:

$$\left[S^T\right] = \begin{bmatrix} \left[S_{11}^T\,(M \times M)\right] & \left[S_{12}^T\,(M \times U)\right] \\ \left[S_{21}^T\,(U \times M)\right] & \left[S_{22}^T\,(U \times U)\right] \end{bmatrix} \tag{3}$$

where $[S_{ij}^T]$ $(i = 1, 2;\ j = 1, 2)$ are complex submatrices, whereas subscripts i and j represent the reception proper modes and the incidence proper modes, respectively. The complex elements of the GSM are the reflection and transmission coefficients (modulus and phase) between proper modes and they give the electromagnetic behaviour of the complete structure under analysis. To perform the spectral analysis, the reformulated algorithm was implemented in the updated software package Telcont. The general flow diagram of the Telcont software package is shown in Appendix A.

3. RESULTS

As mentioned, any refractive index function can be assigned in the optical waveguide cover. This modification makes possible not only the evaluation of evanescent field optical sensors designed in

periodical structures, but also the inclusion of microchannels arrays for constituting segmented optical waveguides applied in optical sensing.

Initially and for evaluating the good performance of the extended and updated algorithm, the behaviour of the planar waveguide photonic crystal analyzed in [1] was verified in a wider band of wavelengths. Figure 3 shows the pattern waveguide photonic crystal, consisting of 11 planar optical waveguides connected abruptly. As in the former case, the common physical parameters were as follows: conducting walls cross section dimensions, $(a \times b)$: (25×60) μm; basic modes number: 130; proper modes number: $M = N = P = \ldots = 15$; maximum index increments: $\Delta n = 0.01$; diffusion depths (μm): $h = 5$; wavelength: $\lambda = 1\,\mu$m; index profile functions of planar waveguides: exponential; waveguide lengths (μm): l_i $(i = 2, 3, 4, \ldots, 10) = l$. The substrate refraction index, n_s, is used as lattice periodic parameter, whereas the waveguide lengths, l, are the lattice constant. All optical waveguides are strongly monomode. We assign, as substrate refractive index, $n_{se} = 2.0$ for odd order waveguides, while $n_{so} = 4.0$ is assumed for even order waveguides. Now, the optical waveguide cover index, n_c, can be chosen as desired. The analyzed wavelength interval was (0.87–1.35) μm. Figure 4 shows the modulus and phase of the reflection, R, and transmission, T, coefficients for the fundamental proper mode, when lattice constant $l = 1.08\,\mu$m. The shaded areas indicated in Figures 4(a), (b) correspond to the results obtained in the first version of the method, which are perfectly reproduced by the current version.

Figure 4 shows four Photonic Band Gaps (PBGs) in the wavelength intervals: (0.915–0.935) μm; (0.99–1.01) μm; (1.155–1.195) μm; (1.275–1.33) μm. In these wavelength regions all the power is reflected, so the periodical structure works as a quadruple photonic mirror (*off states*) in these intervals. However, for wavelengths in the intervals (0.944–0.977) μm and (1.21–1.265) μm all the power is transmitted; so, the structure performs as a double photonic window (*on states*). The phase results for the reflection coefficient, R, are included in Figure 4(b) to verify its monotone variation inside the PBGs, unlike it happens outside of PBGs, where phase changes abruptly.

When a defect breaks the periodicity of the structure, *on states* can be induced in the photonic mirror zones [1]. For example, a single defect can be created by modifying the length or/and the refractive index of an optical waveguide. In both cases, the optical path length is modified, making possible the rupture of the PBG. In order to verify the new version of the algorithm, a local defect was introduced by changing de length of waveguide number 6 in the periodical structure of the Figure 3, so that $l_6 = 1.5147\,\mu$m.

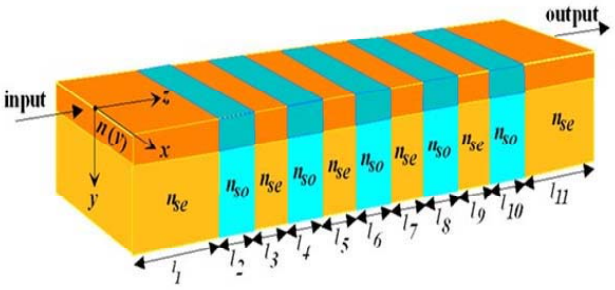

Figure 3. Waveguide photonic crystal in planar optical waveguide, as in [1] but including an arbitrary refractive index, n_{cover}, in the cover region.

Figure 5 shows the creation of one state in each PBG, for wavelengths (μm): $\lambda_1 = 0.934$, $\lambda_2 = 1$, $\lambda_3 = 1.202$ and $\lambda_4 = 1.314$. In these wavelengths, the optical power is totally transmitted, and the structure behaves as an optical microcavity. Again, the phase results, are included. We can see its monotone variation inside the PBGs, except at the wavelength where each PBG breaks. As in Figure 4, the area indicated in Figure 5 matches to the results in [1], ratifying the goodness of the new algorithm. As explained, a similar behaviour can be found modifying the substrate refractive index of the waveguide. This can be seen in Figure 6, for the same structure analyzed in Figure 5, but using the substrate refractive index of waveguide number 6 as parameter. The exploration is focused in the second PBG wavelength region (0.99–1.01) μm. We can see that only a wavelength of the PBG is transmitted for each substrate refractive index, so that this wavelength increases when the substrate

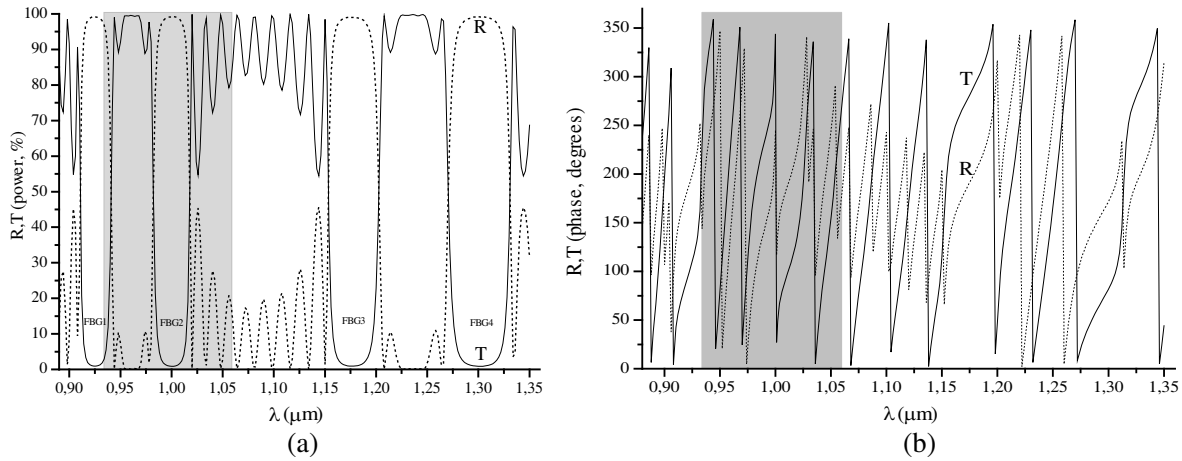

Figure 4. Power (a) and phase (b) for the reflected, R, and transmitted, T, coefficients, versus wavelength, for the fundamental proper mode when lattice constant $l = 1.08\,\mu\text{m}$. The shaded areas compare the new results with the obtained in [1].

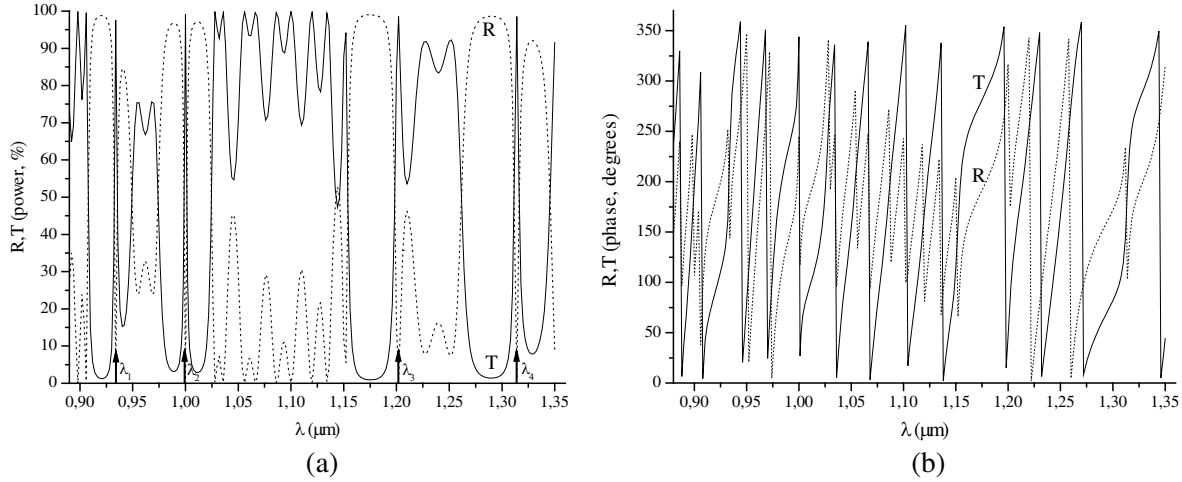

Figure 5. Power (a) and phase (b) for the reflected, R, and transmitted, T, coefficients, versus wavelength, for the fundamental proper mode in the waveguide photonic crystal when a local defect is introduced in waveguide number 6 ($l_6 = 1.5147\,\mu\text{m}$).

refractive index, n_{06}, does it. These results confirm the possibility of using these periodical structures for refractive index sensors design, as it was advanced in [1].

When a refractive index different to the air is used as optical waveguides cover, the global behaviour of the periodical structure remains almost unchangeable but displaced in wavelength. This is demonstrated in Figure 7 for the same planar waveguide photonic crystal analyzed in Figure 4, but using the refractive index of the cover, n_c, as a parameter. As the n_c increases, the PBGs tends to move to lower wavelengths.

The results obtained lead us to analyze the possibility of designing optical sensors combining planar optical waveguides in cascade with microchannels engraved in the same substrate. Different designs can be proposed. We present here the results obtained for the structure shown in Figure 8: planar optical waveguides separated by microchannels. In order to seal the microchannels and to make possible the use of different waveguide covers, a material of refractive index n_c is placed in the top of the periodical structure. From the electromagnetic propagation point of view, this proposal can be asimilated to the case of a segmented planar optical waveguide. As it is known, a segmented optical waveguide can be

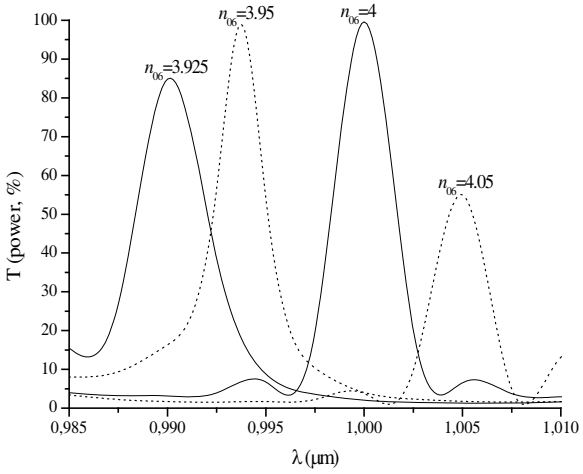

Figure 6. Percentage transmitted power, T, for the fundamental proper mode in the waveguide photonic crystal when a local defect is introduced in waveguide number 6 ($l_6 = 1.5147\,\mu$m), and using as parameter the substrate refractive index of the waveguide 6, n_{06}. The rest of the wavelengths in this second PBG are reflected.

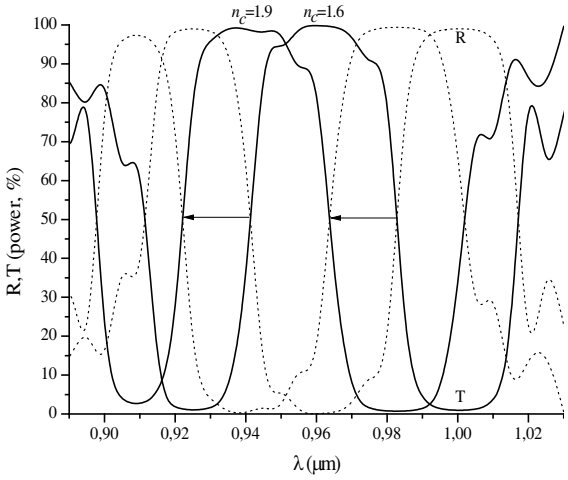

Figure 7. Reflected, R, and transmitted, T, power, versus wavelength, for the fundamental proper mode in the planar waveguide photonic crystal of Figure 3, and using as parameter the refractive index, n_c, of the waveguide covers.

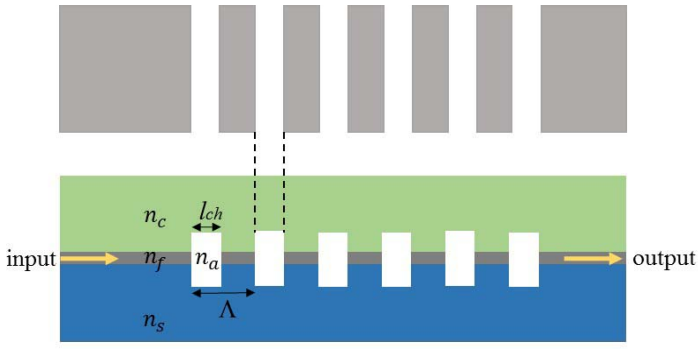

Figure 8. Top (above) and side (below) views of planar optical waveguides separated by microchannels in cascade.

taken as equivalent to an optical waveguide with an average refractive index [30]. In the present case, an analyte flows trough the microchannels in order to know its refractive index by evaluating the scattered light, reflected and transmitted, by the complete structure.

In Figure 8, n_s, n_f, n_c and n_a represent the refractive index in substrate, core, cover and analyte inside the microchannels, respectively, whereas l_{ch} and Λ are the width and period of the microchannels. Initially and in order to explore the electromagnetic behaviour of these structures, two configurations of segmented optical planar waveguides with microchannels were designed. In both cases, the substrate and cover materials were glass (soda lime) and polymer (PDMS), since they are materials commonly used in optics, with well-known physical properties. On the one hand, and with the aim of working with monomode optical planar waveguides, the assigned values to the physical parameters were as follows: $n_s = 1.512$, $\Delta n = 0.01$, refractive index function of guiding region: *exponential*, $h = 2\,\mu$m and n_c=1.40. On the other hand, $l_{ch} = 50\,\mu$m and $\Lambda = 100\,\mu$m, whereas the analyte refractive indices were: $n_a = 1.24, 1.32, 1.40$ ($\Delta n_a = 0.08$). Figures 9 and 10 show the reflected, R, and transmitted, T, powers, versus wavelength, for the fundamental proper mode when using 3 and 15 microchannels, respectively. In both cases, $\Delta\lambda = 0.01\,\mu$m was assigned as lambda increment in the mathematical simulation.

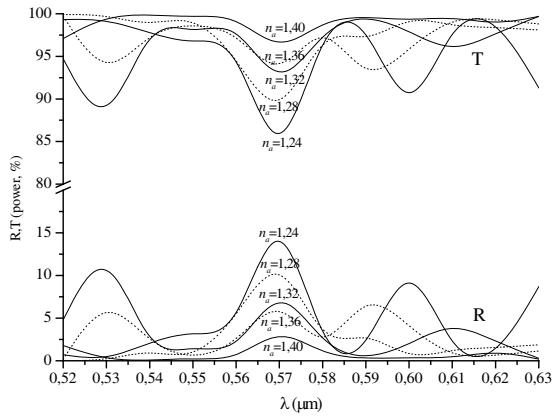

Figure 9. Reflected, R, and transmitted, T, power, versus wavelength, for the fundamental proper mode in the optical waveguide sensor, using 3 microchannels and the refractive index of the analyte, n_a, as parameter.

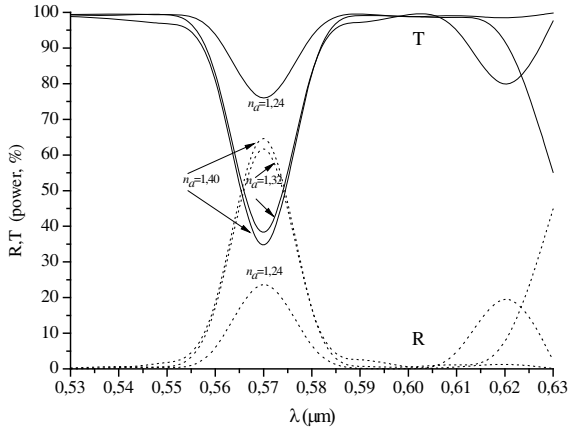

Figure 10. Reflected, R, and transmitted, T, power, versus wavelength, for the fundamental proper mode in the optical waveguide sensor, using 15 microchannels and the refractive index of the analyte, n_a, as parameter.

The results in Figure 9 show that increasing the refractive index of the microchannels, the transmission is clearly improved at certain wavelengths. In this case, it is specially remarkable at $\lambda = 0.57\,\mu\text{m}$, where the structure is specially sensitivy. This behaviour can be explained because as the microchannel index increases, the discontinuity between the optical waveguides and the microchannels is reduced, leading to an increase in the transmitted power. In Figure 10, we can see how the effect of increasing the number of microchannels influences the behaviour of the device. As in Figure 9, and at $\lambda = 0.57\,\mu\text{m}$, the structure presents very interesting results. Again, the transmission improves when increasing the refractive index of the microchannels but, in this case of 15 microchannels, the transmitted power is strongly reduced respect to the previous case. This is due to the strong increment of the number of the abrupt discontinuities, which reduces transmission and increases reflection. Notice that in all cases, the power conservation is excellent. These results show that planar waveguides segmented with microchanels could be used for sensing applications, as for example refractive index sensors and biosensors.

In order to explore in depth the behaviour of these devices, new results were obtained for segmented structures designed with 7 and 15 microchannels. The simulation was performed in the wavelength range (0.54–0.58) μm, but using as lambda increment, $\Delta\lambda = 0.001\,\mu\text{m}$. In both cases, the physical parameters were: $n_s = 1.512$, $\Delta n = 0.01$, refractive index function of guiding region: *exponential*, $h = 2\,\mu\text{m}$, $l_{ch} = 50\,\mu\text{m}$, $\Lambda = 100\,\mu\text{m}$ and $n_a = 1.24$. Figures 11 and 12 show the obtained results. In both cases, the reflection and transmission peaks appear at the same wavelengths; however, for the case of 15 microchannels the reflection and transmission are strongly increased and reduced, respectively, with respect to the device with 7 microchannels. This can be seen at some discrete wavelengths, for example: $\lambda = 0.545\,\mu\text{m}$, $\lambda = 0.555\,\mu\text{m}$, etc. Hence, the number of microchannels mainly influences the magnitude of R and T, without modifying the wavelengths in which these coefficients show a significative behaviour with respect to the rest of wavelengths.

In order to investigate both the efficiency of the algorithm as well as the behaviour and sensitivity of these periodical configurations, when very small changes of the refractive index are introduced, new simulations were carried out. For this purpose, planar segmented waveguides with 15 microchannels were analyzed for two different refractive indexes of the analyte: $n_a = 1.20$ and $n_a = 1.24$. Figure 13 shows the obtained results. As mentioned, when the number of microchannels is increased, the number of refused wavelengths increases as well as the modulus of the reflected power. In this situation, and according with the power conservation, the transmission is reduced.

Electromagnetic windows and mirrors appear periodically located at specific wavelengths, as shown in Figure 13. When the refraction index of the analyte is increased, the number of wavelengths with high

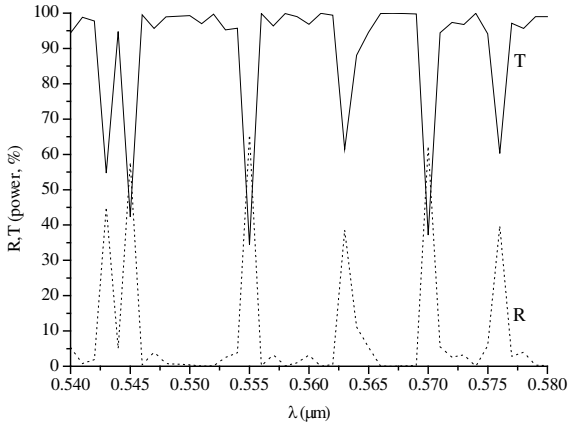

Figure 11. Reflected, R, and transmitted, T, power, versus wavelength, for the fundamental proper mode in the segmented optical waveguide with 7 microchannels and $n_a = 1.24$.

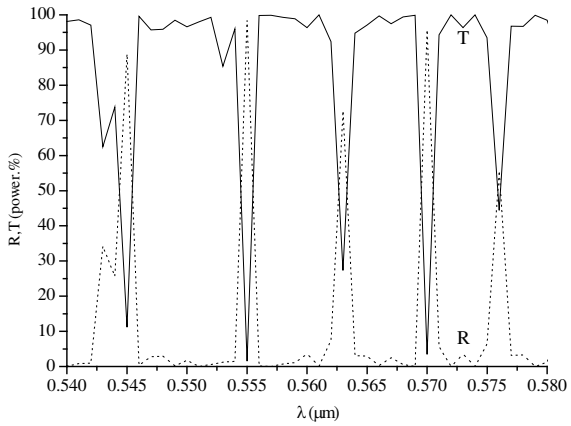

Figure 12. Reflected, R, and transmitted, T, power, versus wavelength, for the fundamental proper mode in the segmented optical waveguide with 15 microchannels and $n_a = 1.24$.

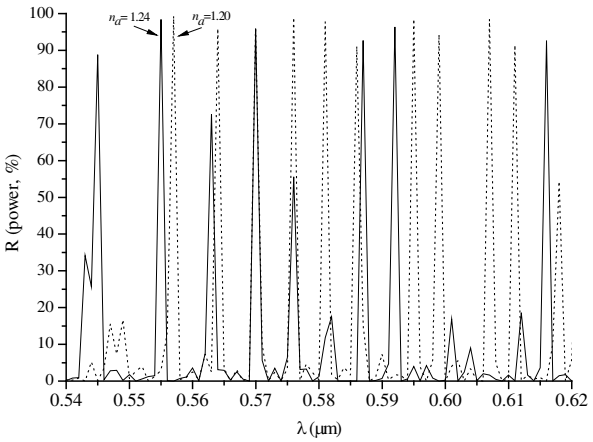

Figure 13. Reflected power percentages comparison, for the fundamental proper mode in the segmented optical waveguide, with 15 microchannels and using the refractive index of the analyte, n_a, as parameter.

reflection is reduced, being suppresed some of them. In the present case, there are ten wavelengths with $R > 80\%$ when $n_a = 1.20$, whereas only five wavelengths with $R > 80\%$ are obtained when $n_a = 1.24$. These results are in agreement with the fact that by increasing the refractive index of the analyte, there is a better adaptation of the refractive indexes at the succesive abrupt optical waveguide-microchannel interfaces.

4. CONCLUSION

The new scattering matrix procedure is a powerful tool in order to analyze the spectral behaviour of integrated optical waveguides in cascade and with arbitrary refractive index in the cover. The inclusion of different optical waveguide cover mediums, as well as engraved microchannels, open the possibility to design refractive index optical sensors and biosensors in the search for future applications and benefits. Multiple photonic band gaps can be obtained for planar waveguide photonic crystals properly designed. The introduction of a defect can create an optical microcavity inside each band gap, allowing total transmission for a specific wavelength. The possibility of being able to use any refractive index of the cover in the algorithm leads to important conclusions. On the one hand, significant shifts of all the

PBG occur for certain values of the refractive index of the cover. On the other hand, the possibility of designing, for the first time, optical sensors based on the simultaneous action of the evanescent field and electromagnetic scattering at the interfaces, in order to increase sensitivity, was confirmed. To do this, a new optical device performed with planar optical waveguides and microchannels in cascade was proposed. The module and the phase of the reflection and transmission coefficients were obtained for several structures, as a function of the wavelength, and using as parameters the optical waveguides and microchannels number, as well as the analyte refractive index. In all cases the power conservation was excellent, and the potential of these structures is highly remarkable for future designs of high sensitivity optical sensors.

APPENDIX A.

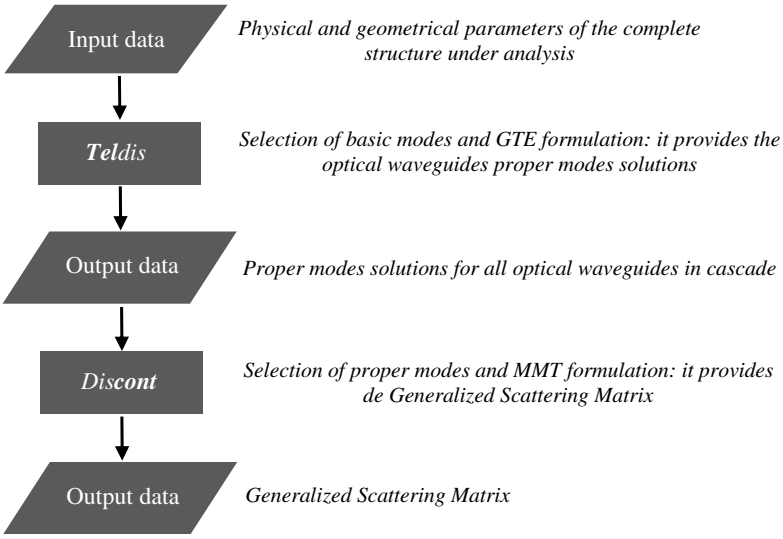

Figure A1. Main modules and flow diagram of the Telcont software package.

ACKNOWLEDGMENT

This work has been supported by the University of Oviedo, under Project PAPI-17-PEMERG-9, and by the Spanish Government, under Project MINECO: CTQ2017-86994-R.

REFERENCES

1. Rodríguez, J., M. G. Granda, A. F. Gavela, S. J. A. Presa, M. R. Lastra, and S. F. Fernández, "Electromagnetic waves scattering at interfaces between dielectric waveguides: A review on analysis and applications," *Progress In Electromagnetics Research B*, Vol. 37, 103–124, 2012.
2. Halir, R., et al., "Waveguide sub-wavelength structures: A review of principles and applications," *Laser Photonics Rev.*, Vol. 9, No. 1, 25–49, 2015.
3. Alberucci1, A., et al., "Light confinement via periodic modulation of the refractive index," *New Journal of Physics*, Vol. 15, 083013, 2013.
4. Bhuvaneshwaran, A., et al., "Spectral response of Bragg gratings in multimode polymer waveguides," *Applied Optics*, Vol. 56, No. 34, 9573–9582, 2017.
5. Ortega, D., et al., "Cutoff wavelength of periodically segmented waveguide in Ti:$LiNbO_3$," *J. Lightwave Technology*, Vol. 16, No. 2, 284–290, 1998.
6. Chang-Hasnain, C. J. and W. Yang, "High-contrast gratings for integrated optoelectronics," *OSA, Advances in Optics and Photonics*, Vol. 4, No. 3, 379–440, 2012.

7. Hopman, W. C. L., et al., "Quasi-one-dimensional photonic crystal as a compact building-block for refractometric optical sensors," *IEEE Journal of Selected Topics in Quantum Electronics*, Vol. 11, No. 1, 11–16, 2005.
8. Lumeau, J., et al., "Micromirrors with controlled amplitude and phase," *Applied Optics*, Vol. 56, No. 20, 5655–5660, 2017.
9. Lambeck, P. V., "Integrated optical sensors for the chemical domain," *Institute of Physics Publishing. Measurement Science and Technology*, Vol. 17, R93–R116, 2006.
10. Kehl, F., et al., "Design of a label-free, distributed Bragg grating resonator based dielectric waveguide biosensor," *Photonics*, Vol. 2, 124–138, 2015.
11. Sahoo, P. K., et al., "High sensitivity guided-mode resonance optical sensor employing phase detection," *Nature Scientific Reports*, 1–7, 2017.
12. Dutta, et al., *Planar Waveguide Optical Sensors. From Theory to Applications*, Chapter 2, Springer International Publishing, 2016, ISBN 978-3-319-35140-7.
13. Taleb, H. and M. K. Moravvej-Farshi, "Designing a low-threshold quantum-dot laser based on a slow-light photonic crystal waveguide," *Applied Optics*, Vol. 56, No. 35, 9629–9636, 2017.
14. Delonge, T. and H. Fouckhardt, "Integrated optical detection cell based on bragg reflecting waveguides," *Journal of Chromatography A*, Vol. 716, 135–139, 1995.
15. Veldhuisy, G. J., et al., "An integrated optical Bragg-reflector used as a chemo-optical sensor," *Pure Appl. Opt.*, Vol. 7, L23–L26, 1998.
16. Parker, R. M., et al., "An integrated optofluidic Bragg grating device to measure the dynamic composition of a fluid system," *OSA/CLEO/QELS*, 2010.
17. Calixto, S., et al., "Diffraction grating-based sensing optofluidic device for measuring the refractive index of liquids," *Opt. Express*, Vol. 24, No. 1, 180–190, 2016.
18. Neustock, L. T., et al., "Optical waveguides with compound multiperiodic grating nanostructures for refractive index sensing," *Journal of Sensors*, Article ID 6174527, 11 pages, 2016.
19. Hong, Y.-S., et al., "Characterization of a functional hydrogel layer on a silicon-based grating waveguide for a biochemical sensor," *Sensors*, Vol. 16, No. 914, 1–9, 2016.
20. Pottier, P., et al., "Quasi-one-dimensional photonic crystal as a compact building-block for refractometric optical sensors," *IEEE Journal of Selected Topics in Quantum Electronics*, Vol. 11, No. 1, 11–16, 2005.
21. Taya, S. A. and S. A. Shaheen, "Binary photonic crystal for refractometric applications (TE case)," *Indian Journal of Physics*, Vol. 92, No. 4, 519–527, 2018, Doi: https://doi.org/10.1007/s12648-017-1130-z.
22. Chen, Y., et al., "Planar photonic crystal based multifunctional sensors," *Applied Optics*, Vol. 56, No. 6, 1771–1780, 2017.
23. Sun, F., et al., "Ultra-compact air-mode photonic crystal nanobeam cavity integrated with bandstop filter for refractive index sensing," *Applied Optics*, Vol. 56, No. 15, 4363–4368, 2017.
24. Sagar, H. P., et al., "Transient dynamic distributed strain sensing using photonic crystal waveguides," *Applied Optics*, Vol. 56, No. 28, 7877–7885, 2017.
25. Ramanujam, N. R., et al., "Enhanced sensitivity of cancer cell using one dimensional nano composite material coated photonic crystal," *Microsystem Technologies*, 1–8, 2018, Doi: https://doi.org/10.1007/s00542-018-3947-6.
26. Taya, S. A., et al., "Photonic crystal with epsilon negative and double negative materials as an optical sensor," *Optical and Quantum Electronics*, Vol. 50, No. 5, 222-1–222-11, 2018, Doi: 10.1007/s11082-018-1487-z.
27. Weissman, Z. and A. Hardy, "Modes of periodically segmented waveguides," *Journal of Lightwave Technology*, Vol. 11, No. 11, 1831–1838, 1993.
28. Ortega, D., et al., "Analysis of "Quasi-Modes" in periodic segmented waveguides," *Journal of Lightwave Technology*, Vol. 17, No. 2, 369–375, 1999.
29. Aschieri, P. and A. Picozzi, "Complex behaviour of a ray in a Gaussian index profile periodically segmented waveguide," *J. Opt. A Pure Appl.*, 386–390, 2006.

30. Rubio-Mercedes, C. E., et al., "Analysis of straight periodic segmented waveguide using the 2-D finite element method," *Journal of Lightwave Technology*, Vol. 32, 11, 2163–2169, 2014.
31. Sharma, M., et al., "Periodically-segmented liquid crystal core waveguides," *J. Phys. D: Appl. Phys.*, Vol. 50, 1–5, 2017.
32. Weissman, Z. and I. Hendel, "Analysis of periodically segmented waveguide mode expanders," *Journal of Lightwave Technology*, Vol. 13, No. 10, 2053–2058, 1995.
33. Tomljenovic-Hanic, S. and J. D. Love, "Planar waveguide add/drop wavelength filters based on segmented gratings," *Microwave and Optical Technology Letters*, Vol. 37, No. 3, 163–165, 2003.
34. Weissman, Z., "Evanescent field sensors with periodically segmented waveguides," *Applied Optics*, Vol. 36, No. 6, 1218–1222, 1997.
35. Weissman, Z., et al., "Mach-Zehnder type, evanescent-wave bio-sensor, in ion-exchanged glass, using periodically segmented waveguide," *SPIE Conference on Specialty Fiber Optics for Medical Applications, San Jose, California, SPIE*, Vol. 3596, 210–216, 1999.
36. Weissman, Z., et al., "Segmented waveguides and their applications for biosensing," *Integrated Optics Devices IV, Giancarlo C. Righini, Seppo Honkanen, Proceedings of SPIE*, Vol. 3936, 284–292, 2000.
37. Van Lith, J., et al., "The segmented waveguide sensor: Principle and experiments," *Journal of Lightwave Technology*, Vol. 23, No. 1, 355–363, 2005.